

Instabilities in Granular Flows

Shaun Hendy

IRL Applied Maths,
Industrial Research Ltd,
P O Box 31-310, Lower Hutt,
New Zealand
s.hendy@irl.cri.nz

April 14, 2024

1 Introduction

The flow and handling of granular materials is of major importance to many industries. Yet despite efforts over several decades, the modeling of such flows has achieved only modest success. Dense gravity-driven flows in hoppers have been often modeled as elastic-plastic continua, for example. In this picture, the granular material flows as a plastic with a frictional yield condition, and deforms as an elastic solid otherwise. This model has been used to analyze mass flows, where the material is flowing throughout the hopper, but has failed to provide adequate agreement with experiment in the prediction of quantities such as discharge rate, for example [17]. Despite such shortcomings, Jenike's [6] construction of steady-state incompressible rigid-plastic radial solutions in hoppers with simple geometries has been of considerable importance in hopper design [10]. These are solutions for quasistatic flow (inertial effects are neglected) where grains travel radially in conical or wedge-shaped hoppers. Only recently have numerical solutions of steady-state quasistatic flows in more complicated geometries been produced [5].

However, it is now clear that there are serious mathematical difficulties with the equations for time-dependent incompressible rigid-plastic flow (IRPF). In many instances, the equations for such flows have been shown to be ill-posed i.e. they possess instabilities with arbitrarily short wavelengths (Schaefer [12], Valanis and Peters [18]). Hence, it is problematic to interpret the steady-state rigid-plastic flow equations as long-time solutions of the time-dependent equations. Additionally, both the steady-state and time-dependent equations have physical shortcomings. There are several features of hopper flows where the particle size is important, indicating that it may not be appropriate to model such dense granular flows as continua.

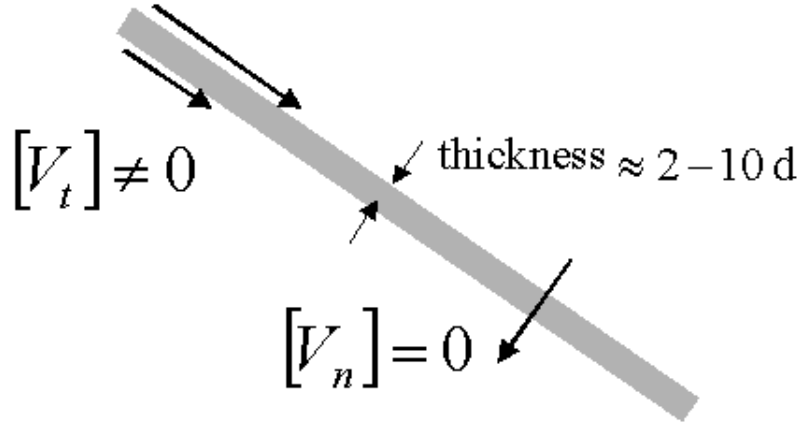


Figure 1: Schematic illustration of shear banding. In granular materials the band is typically several grain diameters (d) thick.

One flow feature that involves the particle size is that of shear-banding. Shear-banding is an extremely interesting phenomena that occurs in plastically deforming materials, including granular materials. At high strains the deformation of the material becomes localized in thin bands of shearing. This leads to a jump in velocity across the band as illustrated in figure 1. In granular flows, the thickness of this band is typically only several grains thick, yet the length can be comparable to the size of the container. Thus shear-banding in granular flows seems to be a flow feature that spans both the kinetic and the hydrodynamic regimes. In this sense, shear-banding in granular materials differs, for example, from the discontinuities encountered in compressible fluid flows where shocks are smoothed by hydrodynamic effects (e.g. viscosity). The full theory of granular flow ought to predict a shear band thickness of zero in the hydrodynamic limit.

It is probable that a complete description of shear-banding in granular flows is not within the scope of a continuum theory. Nonetheless, attempts have been made to describe shear-banding in continuum theories in some average sense ([9]). Indeed, continuum plastic flow theories have been found to exhibit shear-banding type behavior and the development of shear-bands seems to be closely related to the development of ill-posedness in such flows [14]. One approach to deal with ill-posedness is to model the granular material as a Cosserat continua. Cosserat-type continuum theories attempt to model materials with internal structure by the inclusion of extra terms motivated by physics at the granular scale. These extra terms can damp the instabilities that lead

to ill-posedness and can be used to predict shear-band thickness (Mühlhaus [9]). Including such damping terms which act at a granular length-scale and ‘thickening’ the shear-bands is a practical approach to studying granular flows using continuum equations. Indeed, such an approach is analogous to including Reynolds stresses in the Navier-Stokes equations to model turbulence.

The purpose of this paper is to study a set of equations for granular flow, which are a simple generalization of the IRPF equations, and which display shear-banding instabilities similar to those that arise in the Critical State theory (CST) of granular flow [13]. These equations appear to be more regular than the full IRPF equations and are somewhat simpler than CST-motivated equations. We do not explicitly introduce a granular length scale here; we wish to study the development of shear-banding from a hydrodynamic viewpoint. In the first section we state the usual equations for IRPF. In the next section, we review the linear stability analysis of these equations and show that they are linearly ill-posed in two dimensions. In section four, we introduce a new set of equations which are a singularly perturbed form of the IRPF equations, and in the next section we present numerical solutions of these equations which demonstrate shear-banding. Finally, we look at the linear stability of these equations to provide a qualitative description of the shear-banding process.

2 Equations for an incompressible rigid-plastic flow

We consider the flow under gravity of an incompressible granular material in a wedge-shaped hopper under plane strain. We model the flow of this material as a continuum rigid-plastic flow. The equations for such a flow consist of the incompressibility condition,

$$r_i u^i = 0 \quad (1)$$

where u^i are the components of the velocity field, and the momentum equations:

$$\frac{\partial u^i}{\partial t} + u^j r_j u^i + r_j{}^{ij} = g^i; \quad (2)$$

where r_{ij} is the symmetric stress tensor, and g^i is the acceleration due to gravity. Note that we define to be positive when forces are compressive.

Plastic deformation is assumed to occur everywhere in the hopper i.e. the material is at plastic yield throughout the hopper. We will use a flow rule based on a Ducker-Pager type yield condition [4]. Specifically, in terms of the principal stresses σ_i , this condition is written as

$$(\sigma_1 - \sigma_2)^2 + (\sigma_2 - \sigma_3)^2 + (\sigma_3 - \sigma_1)^2 \leq k^2 \quad (3)$$

where $k = \frac{p}{2} \sin \phi$, ϕ is the internal angle of friction of the material and $\bar{\sigma} = \frac{1}{3}(\sigma_1 + \sigma_2 + \sigma_3)$ is the average trace of the stress tensor (we will refer to as the average stress). If this inequality is satisfied exactly then the material is

deforming plastically. Under plane strain $\epsilon_2 = \epsilon_3 = \frac{1}{2}(\epsilon_1 + \epsilon_3)$, so in this case we may consider a strictly two-dimensional yield condition:

$$(\epsilon_1 - \epsilon_2)^2 + (\epsilon_3 - \epsilon_2)^2 = 2\sigma^2 \sin^2 \alpha, \quad (4)$$

We now assume a flow rule of the form

$$\dot{\epsilon}_{ij} = \dot{\epsilon}_{ij} + V_{ij}; \quad (5)$$

where $V_{ij} = (\dot{\epsilon}_i u_j + \dot{\epsilon}_j u_i)/2$ and $\dot{\epsilon}$ is some, as yet unspecified, scalar function of the normal stress and strain rates. If we compare the flow rule (5) to the yield condition (3), then we see such a flow will satisfy the yield condition exactly if we choose the function $\dot{\epsilon}$ to be

$$\dot{\epsilon} = \frac{k}{\sqrt{V_{ij} V^{ij}}}; \quad (6)$$

where $\sqrt{V_{ij} V^{ij}} = \sqrt{\frac{1}{2} V_{ij} V^{ij}}$.

Equations (1), (2), (5) and (6) form a closed system for incompressible rigid-plastic flow in plane strain. For granular flows in hoppers, these equations are only valid for so-called mass flows where the material is flowing throughout the hopper. When the hopper is not sufficiently steep funnel flows can develop where material flows down a central funnel leaving a stagnant region adjacent to the walls. Indeed, radial solutions have been used to study the transition between mass and funnel flow which is thought to occur when the rigid-plastic equations become singular as the rate of deformation vanishes [3]. We will restrict our attention to mass flows where rigid-plastic flow occurs everywhere in a given domain.

On each wall of a hopper, the direction of flow is tangent to the wall and the stresses must satisfy a Coulomb friction condition. The Coulomb boundary condition in two dimensions can be written as follows:

$$\dot{\epsilon}_{ij} n^i t^j = \tan \alpha_w \dot{\epsilon}_{ij} n^i n^j; \quad (7)$$

where \mathbf{n} is a outward-pointing normal vector to the wall, \mathbf{t} is a tangent vector to the wall pointing in the opposite direction to that of the flow and α_w is the angle of wall friction.

Combining equations (1), (2), (5) and (6) together we obtain the equations:

$$\frac{\partial u^i}{\partial t} + u^j r_j u^i = g^i - r_j p^{ij} - k p^{ij}; \quad (8)$$

$$r_i u^i = 0; \quad (9)$$

where

$$p = \frac{1}{2} \sigma^2; \\ A_{ij} = V_{ij} \sqrt{V_{ij} V^{ij}};$$

These equations are strictly hyperbolic in the case of plane strain (equation (5)).

3 Ill-posedness of the incompressible rigid-plastic flow equations

The equations (8) and (9) have been shown to be linearly ill-posed in certain geometries and for certain parameter values [12]. Specifically, the linearized equations of motion that describe the propagation of a small disturbance in the flow, possess unstable plane-wave solutions in the short wavelength limit. It has been suggested that these instabilities are related to the formation of shear bands in the flowing granular material. In this section, we will consider the linearized equations of motion for a plane-wave disturbances to look for ill-posedness. This ill-posedness in the IRPF equations was originally noted by Schaefer [12] for fully three-dimensional flows. Here we will work only in 2D, but with the full linearized equations of motion for a small disturbance. This will serve to provide a comparison with work in the following sections.

We will begin by writing the two-dimensional rigid-plastic equations (8 and 9) in non-dimensional form as follows:

$$\hat{u}^i = u^i/u_0; \hat{p} = p/gL; \hat{x}^i = x^i/L; \hat{t} = tu_0/L; \quad (10)$$

where u_0 is some characteristic velocity and L is some characteristic length-scale of the problem. The equations for the rigid-plastic flow then become

$$\frac{\partial \hat{u}^i}{\partial \hat{t}} + \hat{u}^j \hat{r}_j u^i = \frac{1}{Fr^2} g^i g^h \hat{r}_j \hat{p}^h_{ij} - k \hat{p}^i_{ij} A_{ij}; \quad (11)$$

$$\hat{r}_i \hat{u}^i = 0; \quad (12)$$

where $Fr = u_0 = \frac{p}{gL}$ is the Froude number. At this stage we will drop the $\hat{}$ notation and assume that we are dealing with dimensionless quantities unless otherwise specified.

The linearized equations of motion for a small disturbance $(u; p)$ propagating on a smooth background solution $(u; p)$ to equations (11) and (12) can be shown to be:

$$\frac{\partial u^i}{\partial t} + u^j r_j u^i + u^j r_j u^i = \frac{1}{Fr^2} r_j k p A^{ij} + p A^{ij} - p^{ij}; \quad (13)$$

$$r_i u^i = 0; \quad (14)$$

where

$$A_{ij} = \frac{1}{2} (r_i r_j + r_j r_i) - \frac{r^k r^l}{2V} \frac{\partial u^k}{\partial x^l}; \quad (15)$$

We consider plane-wave disturbances $(u; p) = \exp(i(t + \mathbf{x} \cdot \mathbf{a})) (\mathbf{a};)$ propagating with wavevector \mathbf{a} . In general \mathbf{a} and \mathbf{a} will be complex quantities. From the linearized equations, we obtain the following relations for \mathbf{a} , \mathbf{a} and \mathbf{a} :

$$a_i = B_i + C_{ij} a^j; \quad (16)$$

$$\mathbf{a} = 0; \quad (17)$$

where

$$B_i = \frac{1}{F r^2} k r^j A_{ij} + i(k A_{ij} - i_{ij})^j; \quad (18)$$

$$C_{ij} = (r_j u_i + i(r_j u_i - u_j)) + \frac{1}{F r^2} M_{ijk1} k^k + i r^k (M_{ijk1})^k; \quad (19)$$

and

$$M_{ijk1} = i(j-1)k A_{il} A_{jk}^l;$$

One can solve (16) and (17) for a^i for every wavevector k . The real part of a^i determines the growth or decay of the plane-wave disturbance with wavevector k , and the imaginary part determines the propagation of the disturbance. If the real part of a^i is positive for any k , we refer to this mode as linearly unstable, as this mode will grow rapidly in time. If, for a given background solution, (16) and (17) have unstable modes, then this solution will be termed linearly unstable. If, for a given background solution, there are unstable modes with arbitrarily short wavelengths, and if this background solution is a unique solution of the IPRF equations, then we will call these equations and the solution linearly ill-posed.

Using the condition $a = 0$ we can eliminate a^i from the equation for a^j :

$$a^i = D_{ij} a^j; \quad (20)$$

$$D_{ij} = i k \frac{B_i}{B} \sim C_{kj}; \quad (21)$$

$$= \frac{C_{ij}}{B} \sim i a^j; \quad (22)$$

The eigenvalues of the matrix D (21) determine the growth and propagation of the infinitesimal plane-wave disturbance.

From (21) it can be shown that D has at least one zero eigenvalue $\lambda_1 = 0$. Since we are working in two dimensions, the remaining eigenvalue is equal to the trace of D : $\lambda_2 = \text{Tr}(D)$. This trace is given by

$$\text{Tr}(D) = \text{Tr}(C) \frac{C_{ij} i B^j}{B}; \quad (23)$$

$$= i(a \cdot \tilde{a}) + \frac{i B^j}{B} r_j u_i + A_{ik} r^k A_{j1} + A_{ij-1} A^{lk} q_k + i r_k A^{lk} :$$

where we have used the fact that the matrix is symmetric $A_{ij} = A_{(ij)}$, is trace-free $A_{ii} = 0$ and further that $\text{Tr}(A_{ik} A_{kj}) = 1$.

We now consider the short wavelength ($j \rightarrow 1$) limit of (23). If we write $\tilde{a} = \tilde{a}^j j$ then we can examine the powers of j on the right-hand side of (23). The leading order term in \tilde{a} on the right-hand side goes as $O(j^2)$ and is real with coefficient

$$\frac{(A_{lm} - m)(i k A_{ik})^k A_{ij}^j}{(p q - k A_{pq})^p q} \quad (24)$$

This leading order term was considered by Schaefer ([12]) in his analysis of (8) and (9). The denominator is always positive for angles of friction $\gamma > 0$. The

numerator vanishes when \mathbf{k} points in the direction of the velocity characteristics (these lie at 45° to the principal stress directions) or in the direction of the stress characteristics (these lie at angles of $(\theta' + 90^\circ)/2$ to the principal stress directions) of the background solution. To illustrate this, we have computed the eigenvalue λ_2 for a range of wavevectors for the approximate radial solution (given in the appendix). The results are displayed in figure 2. In this contour plot the four wedges of unstable directions approach those given by (24) in the short wavelength limit.

Plane wave disturbances with wavevectors \mathbf{k} that lie in directions between the stress and velocity characteristic directions will be unstable in the short wavelength limit as the real part of λ_2 will be positive in this limit. This short wavelength instability leads us to conclude that the two-dimensional granular flow equations are linearly ill-posed (this was first noted by Schaeffer [12]).

4 Singularly perturbed rigid-plastic flow equations

Attempts to study (8) and (9) numerically is problematic. Solutions of these equations obtained numerically are found to be grid-dependent due to the wedge of short wavelength instabilities (24) found in the previous section. Here we propose modifying the equations (8–9) in an effort to ‘regularize’ the instabilities (16) in some manner. We will consider the following equations:

$$\frac{\partial u^i}{\partial t} + u^j r_j u^i = g^i - r_j p^{ij} - \kappa p^{ij}; \quad (25)$$

$$r_i u^i = p; \quad (26)$$

These equations are introduced as a tool to study shear-banding rather than an attempt to accurately model the physics of dense granular flows. However, it is worth noting some of the physical properties of these equations. These equations do not conserve mass as the density is held constant despite (26). They do satisfy a Ducker-Peeger yield condition (3) if one assumes a flow rule that is a natural generalization of (5):

$$r_{ij} p_{ij} = (V_{ij} - \text{Tr}(V) \delta_{ij}/2); \quad (27)$$

where δ is given by (6). Now, in this case

$$k^2 p^2 - (r_{ij} p_{ij})^2 = k^2 p^2 (1 - \beta^2/2); \quad (28)$$

where $\beta = p = \mathbf{j} \cdot \mathbf{V} \cdot \mathbf{j}$. Note that equation (26) guarantees that $\mathbf{j} \cdot \mathbf{j} = 2$.

If $\beta = 0$, then the material is at yield and is incompressible, however as p increases the material relaxes from yield. If β is sufficiently small, one might expect that in some instances the solutions of (25) and (26) will approximate smooth solutions of (16–17). Nonetheless, we will see the inclusion of this term significantly alters the behavior of the linearized perturbation equations.

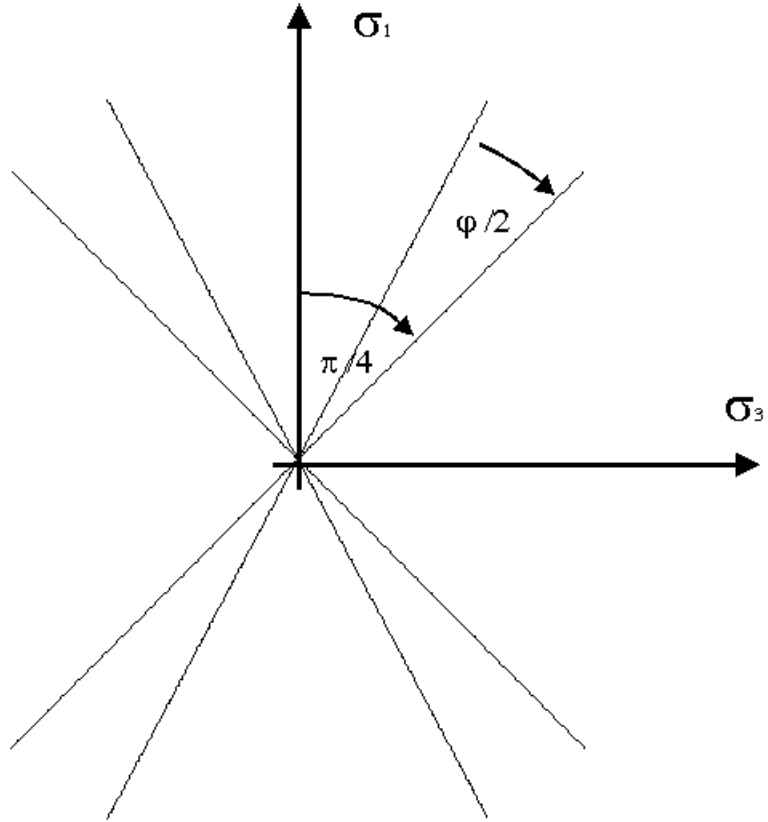


Figure 2: Contour plot of the real part of the eigenvalue σ_2 for the radial solution as a function of wavenumber (radial coordinate) and direction of the wave front (angular coordinate). Inside the wedges σ_2 is positive; outside the wedges, σ_2 is negative.

The equations for plane-wave disturbances analogous to (16-17) are:

$$a_i = B_i + C_{ij}a^j; \quad (29)$$

$$a = \frac{1}{2} : \quad (30)$$

where B and C are given by (18) and (19) respectively. Using (29) we can eliminate directly from (29) to give:

$$a_i = D_{ij}a_j = (C_{ij} - \frac{B_{ij}}{2})a^j; \quad (31)$$

The leading order term on the right-hand side of (31) in the short wavelength limit again goes as $O(j^{-1/2})$. This term is found to be

$$M_{ij} = \frac{1}{F r^2} M_{ijkl} k^k l^l; \quad (32)$$

The first step in analyzing the eigenvalues of D is to look at the eigenvalues of this leading order part M. In what follows we will set $F r = 1$, and ignore the inertial terms which do not play a role in shear banding. If we write

$$M_{ij} = \frac{P}{2j^2}; \quad (33)$$

then the trace of M is given by

$$\text{Tr}(M) = 2 + \frac{P}{2} \cos(2\theta); \quad (34)$$

and the determinant of M is

$$\text{Det}(M) = \frac{1}{2} \left(\frac{P}{2} \cos(2\theta) + 2 \right)^2 - \frac{P^2}{4} \cos^2(2\theta); \quad (35)$$

where θ is the angle of the wavevector to the principal stresses (here the stress is defined by equation (27)), and

$$P = \frac{1}{2} :$$

Noting that $j \sim \frac{1}{2}$, we see the trace of M is always negative. Further, $\text{Det}(M)$ is non-negative (if $j > \frac{1}{2}$ then $\text{Det}(M)$ is strictly positive). Hence the matrix M has no positive eigenvalues, although one of the eigenvalues will vanish in the directions $\cos(2\theta) = -\frac{P}{2}$ provided $j < \frac{1}{2}$. For a smooth background solution with $j \sim 1$, M will have a zero eigenvalue in four directions.

In the short wavelength limit, the eigenvalues of D will tend to those of M (as these grow as $j^{-1/2}$) except in the four directions where the determinant of M vanishes. Thus in this limit D will possess eigenvalues which are negative except very near these four isolated directions. This is in contrast to the earlier situation where equations (13) and (14) possessed a wedge of unstable directions in the short wavelength limit. The possibility still remains that the equations (25) and (26) will be ill-posed near the four directions $\cos(2\theta) = -\frac{P}{2}$.

5 Numerical solutions

In this section we present numerical solutions of the equations (25) and (26). These equations are solved in a two-dimensional wedge-shaped hopper with frictional boundary conditions on the walls ($\mu = \mu_w$) and stress-free inflow/outflow conditions on the arcs $r = r_0$ and $r = r_1$. The radial solution described in the appendix is supplied as an initial condition. These computations have been using a finite element toolkit called Unstructured Grids (UG) which is freely distributed by the IWR at the University of Heidelberg [1].

The equations are discretized using a finite-volume scheme. Finite-volume methods have been successfully used to solve the Navier-Stokes equations in a variety of situations (Patankar [11]). We have chosen to use a control volume finite-element method due to Schneider and Raw (15); see also Karimian and Schneider [7]). This method utilizes colocated primitive flow variables (i.e. average stress and velocities which are discretized on the same grid) so is well suited to the formulation of the incompressible rigid-plastic flow equations presented in the previous section. The equations are discretized in time using a first-order backwards Euler scheme.

The initial difficulty in solving these equations is the non-linearity in the stress terms on the right-hand side of (25). The convective terms in (25) are also non-linear. We will use a Newton linearization of these non-linear terms and solve the resulting equations using a Newton iteration. Within each Newton iteration, the resulting linear problem is solved using a biconjugate gradient method with multigrid preconditioning.

The second difficulty is the growth of the instabilities and the development of shear bands. Once the instabilities develop a small time-step must be used. The shear-banding results in discontinuities developing across the wavefronts that grow from the instability. This is dealt with in an ad hoc manner; the grid is designed so that the discontinuities form parallel to element boundaries. The hopper has been discretized using grids of up to 4000 linear quadrangular elements. These fine grids are required to accurately resolve the right-hand side of (26) when $\mu = 1$. On sufficiently fine grids, one finds that the wavelength of the instability is controlled by the magnitude of μ .

Figures 3 and 4 depict the evolution of the flow from the smooth radial flow solution (see appendix). The figures show flows with $\mu' = 34$ and $\mu'_w = 9^\circ$. The parameter μ is chosen to be $2 \cdot 10^5$. The flows develop as follows:

Initially, plane wave-like wavefronts in the stress develop near the center of the hopper. This region corresponds to the location in the hopper where μ is largest.

At these wavefronts, the tangential velocity component begins to develop jumps across the trough of each wavefront.

These instabilities develop further and further down the hopper, and the formation of jumps in the tangential velocity across the wavefronts follows.

The growth of the wavefronts in amplitude does not increase without bound. Eventually, the growth appears to cut off. The wavefronts are observed to propagate down the hopper (see figure 5 where $\theta' = 34^\circ$ and $\theta_w = 9^\circ$ but λ is $1 - 10^4$ so that the wavelength observed here is longer than in preceding figures). No steady state emerges.

In the next section, we will analyze the linear stability of this system in further detail to try to understand these features. These features very much resemble shear bands, particularly the jumps in tangential velocity that occur across the wavefronts. It should be noted that the thickness across which this jump occurs seems to be grid-dependent. Thus, the shear bands are not fully resolved by the numerical method.

6 Instabilities in the singularly perturbed system

Including the singular perturbation in (26), introduces a new scale, ϵ , to the problem. The grouping $\frac{P}{2} \frac{\partial}{\partial x}$ gives a length-scale that appears in the modified eigenvalue problem (equation 31). Indeed, the wavenumber of the instabilities in the hopper interior that are observed in the numerical studies above roughly satisfy $j \approx \frac{1}{\epsilon}$ so this length-scale appears to be relevant for these features at least. This suggests that the eigenvalues of the following truncation of the full tangent matrix D should be sufficient to study the stability of these unstable modes:

$$D_{ij}^0 = M_{ij} + \frac{1}{\epsilon} (k A_{ik} - \delta_{ik}) \delta_{kj}; \quad (36)$$

This truncation D^0 neglects the imaginary parts of D , and the contribution from the inertial terms.

The trace and determinant of D^0 are given by:

$$\text{Tr}(D^0) = \text{Tr}(M) - \frac{1}{\epsilon} \left(1 + \frac{k}{2} \left(\frac{P}{2} \frac{\partial}{\partial x} \right)^2 \cos(2\theta) \right); \quad (37)$$

$$\text{Det}(D^0) = \text{Det}(M) + \frac{1}{\epsilon} \left((2 - \frac{k}{2}) \cos^2(2\theta) + k \left(\frac{P}{2} \frac{\partial}{\partial x} \right)^2 \cos(2\theta) + \left(\frac{k}{2} \right) \right); \quad (38)$$

In the short wavelength limit $\text{Tr}(D^0) \approx \text{Tr}(M)$ and, unless $\text{Det}(M)$ vanishes, $\text{Det}(D^0) \approx \text{Det}(M)$. If, however, $\text{Det}(M)$ vanishes then

$$\text{Det}(D^0) \approx \frac{2}{\epsilon} \left(\frac{k}{2} \right); \quad (39)$$

so that the determinant of D^0 will be negative if $0 < \theta < k$. In this case D^0 will possess a positive eigenvalue where $\text{Det}(M)$ vanishes. Thus it seems plausible that under certain conditions (25) and (26) can become ill-posed along the directions where $\text{Det}(M)$ may vanish. We should be cautious, however, in

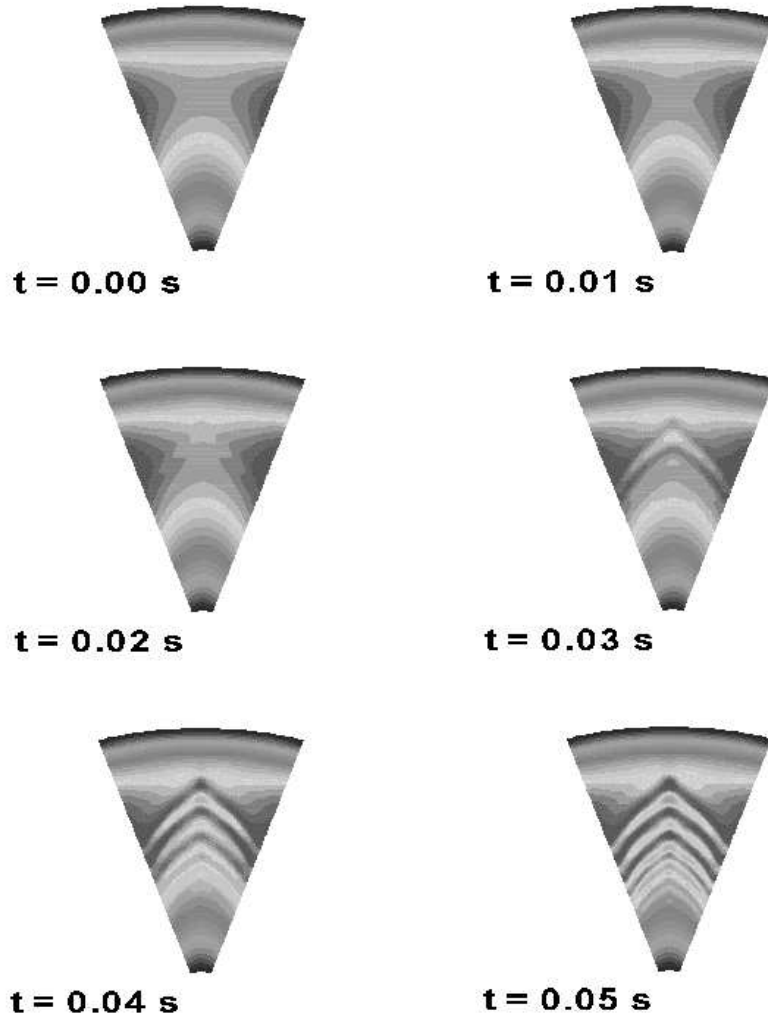


Figure 3: Contour plots of the average stress in a wedge-shaped hopper showing the development of instabilities. Snapshots have been taken at 0.01 s intervals. These instabilities lead to shear banding.

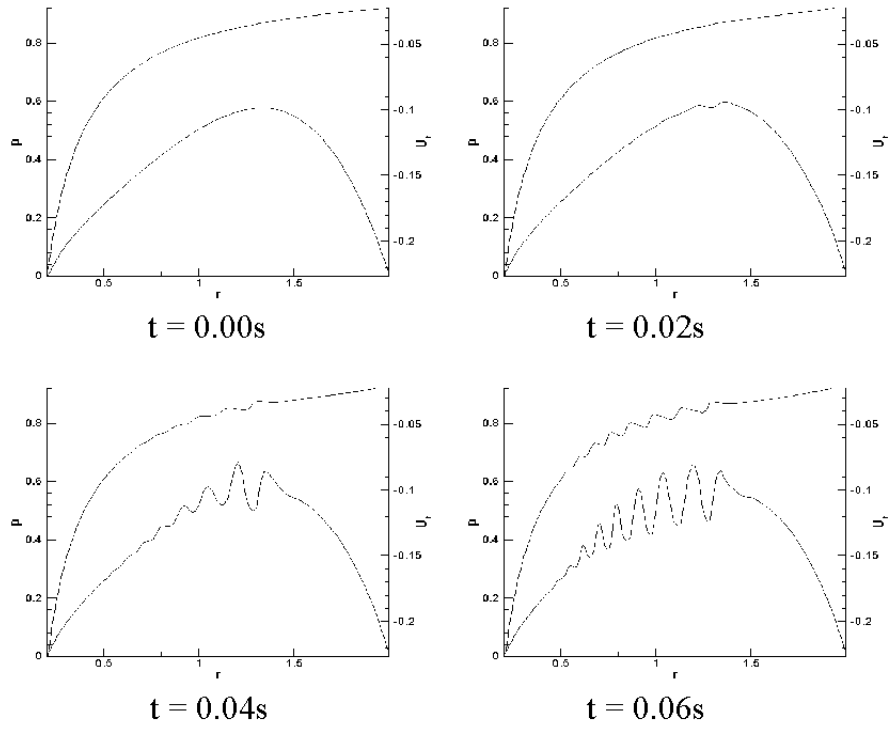


Figure 4: Radial slices (constant θ) of the average stress, and the tangential velocity component across the band. The normal velocity components (not shown) are continuous across the bands. Snapshots are taken at 0.02 s intervals.

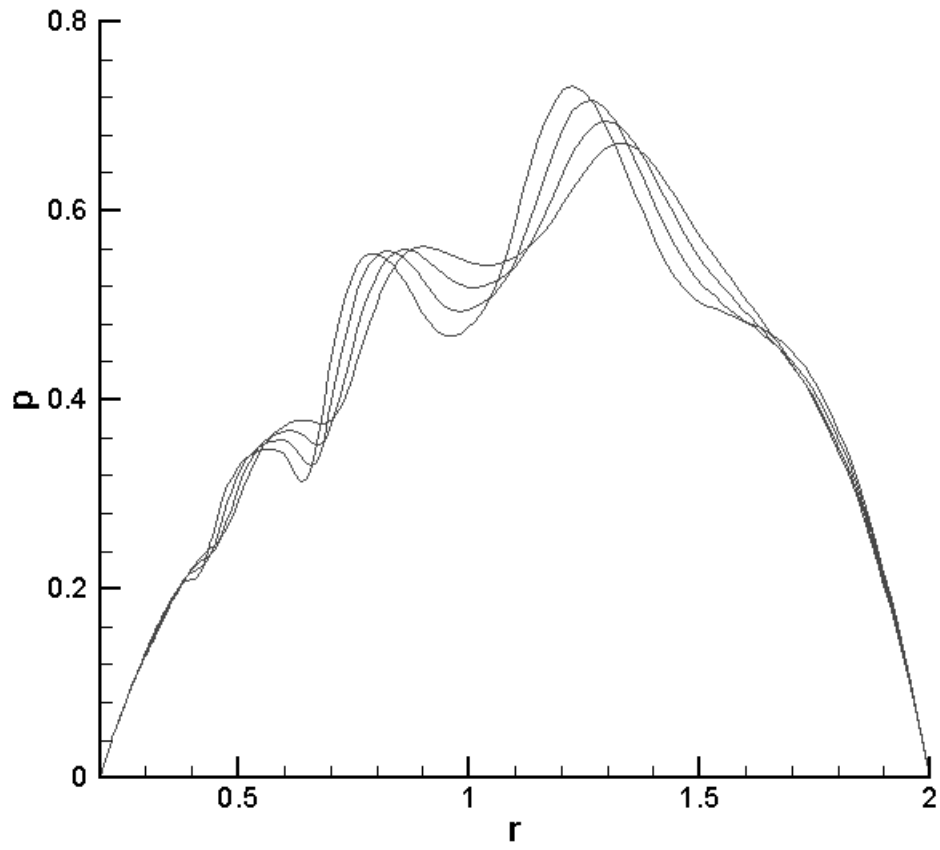


Figure 5: Radial slices (constant θ) of the average stress. This shows the wave-fronts propagating down the hopper. Snapshots are taken at 0.025 s intervals.

drawing conclusions about the short wavelength behavior of D , from the short wavelength behavior of D^0 .

Away from the short wavelength limit, examination of $\det(D^0)$ reveals the possibility of other instabilities. The existence of these instabilities depends on the size and sign of β . There are three possibilities which are classified below:

1. $0 < \beta < \frac{k}{2(\kappa^2 + 1)}$: $\det(D^0)$ is non-negative for all wavenumbers and all directions.
2. $\beta > k$ or $\frac{k}{2(\kappa^2 + 1)} < \beta$: $\det(D^0)$ can be negative for wavenumbers that satisfy
$$0 < k < 2(\kappa^2 + 1) - (\kappa^2 - k) = (\kappa^2 + k):$$

Thus $\det(D^0)$ is non-negative in the short wavelength limit (the problem is linearly well-posed).

3. $k < 0$: $\det(D^0)$ can be negative at any wavelength (i.e. this suggests the problem may be linearly ill-posed).

The situation is illustrated schematically in figure 6.

This provides a qualitative explanation of the development of shear bands observed in the numerical simulations detailed in the previous section. The initial smooth background solution will have small, negative values of β , so the problem is initially well-posed everywhere but unstable to perturbations of wavenumber $j \sim 1/\delta$. As an example, the determinant of the full tangent matrix D has been computed for the radial background solution near the center of the hopper (see appendix), with $\theta = 34^\circ$, $\theta_w = 9^\circ$ and a value of $\beta = 2 \times 10^{-5}$. Illustrated in figure 7, we can see that the unstable region disappears as $j \rightarrow 1$, which is consistent with the behavior of D^0 .

After a short time, an instability does develop with wavenumber $j \sim 1/\delta$ and wavevector at approximately 45° to the directions of principal stress. Once the disturbance grows sufficiently large, equations (29-30) will cease to describe the behavior of the disturbance. Nonetheless, we can continue a qualitative description of the process using (29-30) as a guide. As this disturbance grows then, β becomes a rapidly changing function of position in the hopper. In the troughs of the plane-wave-like pressure disturbance, β is positive, and the linear stability analysis would suggest that the solution becomes ill-posed in this case. Comparing this with the numerical simulations suggests that this ill-posedness in the troughs of the pressure disturbance causes a very strong gradient in the velocities to develop, which in turn drives β to zero. This feedback may provide a mechanism to regularize the ill-posedness. This needs to be studied further, by looking at length scales other than δ and by utilizing a non-linear analysis more suited to dealing with the inhomogeneities that develop as the instabilities grow.

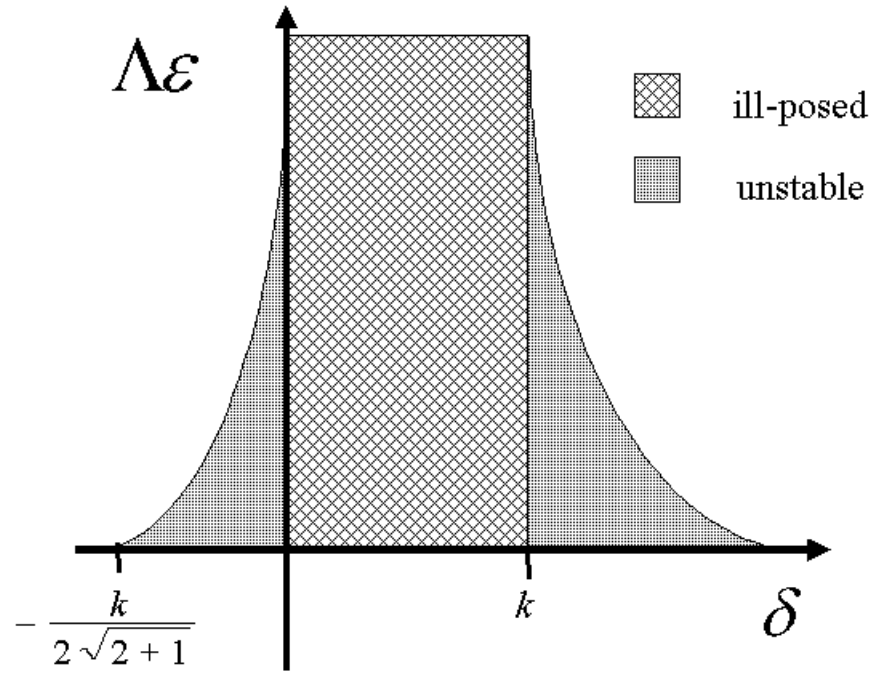


Figure 6: Schematic stability phase diagram in terms of the δ (which depends on frequency) and the parameter $\Lambda \varepsilon$. There is now dependence on the direction of the wavevector in this plot; for points on the plot denoted unstable or ill-posed, there exists at least one direction with this property.

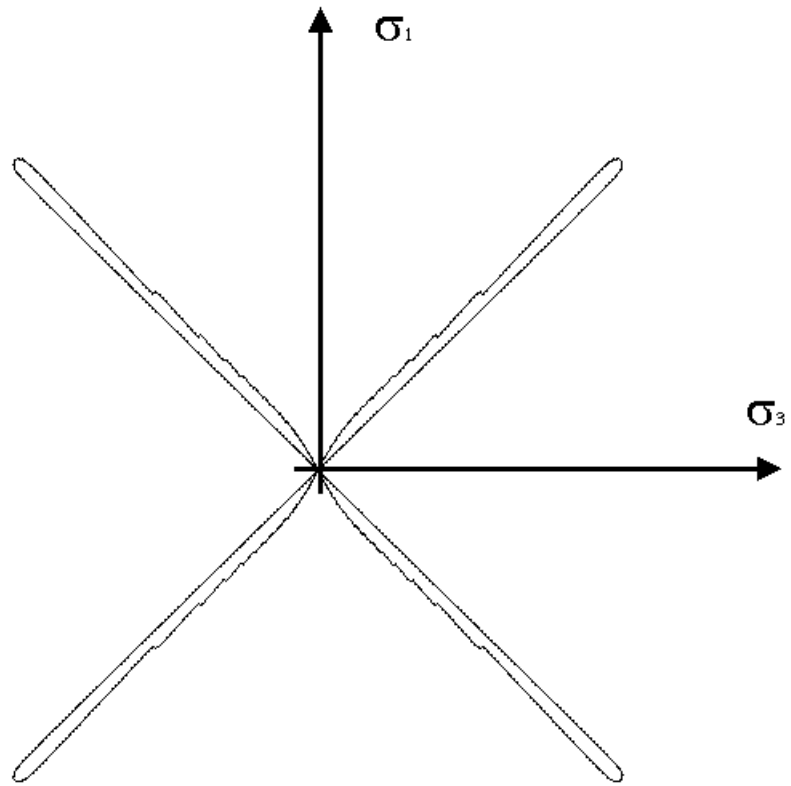


Figure 7: Contour plot of the real part of the eigenvalue σ_2 for the radial solution as a function of wavenumber (radial coordinate) and direction of the wave front (angular coordinate). The contour depicted is the $\sigma_2 = 0$ contour. Inside the contour σ_2 is positive; outside this contour, σ_2 is negative. Here we can see the unstable region disappears as $j \rightarrow 1$.

7 Discussion

We have presented new equations which exhibit shear-banding behavior. These equations are related to the IRPF equations by a singular perturbation. This singular perturbation regularizes the linear ill-posedness inherent in the IRPF equations by collapsing the wedge of wave directions that are unstable in the short wavelength limit. These resulting equations still possess instabilities, related to those of the IRPF as seen in the linear stability analysis, and in numerical simulation these instabilities lead to shear-banding. The linear stability analysis suggests that the inhomogeneity that develops with these instabilities leads to further short wavelength instabilities, which cause these shear-band like features to develop.

The wavelength of the instabilities observed in the singularly perturbed equations was controlled by the time-scale τ . The thickness across the jumps in tangential velocity across the wavefronts was found to be grid-dependent however. The linear stability analysis considered here was concerned with length scales $P^{-1/2}$ and did not predict a thickness across these jumps. However the analysis suggests that they are associated with the ill-posedness that can develop under certain circumstances. It is possible that the thickness of the shear bands here is zero; in this case, it would be impossible to fully resolve the band numerically. Indeed, we were not able to resolve the bands in our numerical simulation. However, the linear analysis does suggest a mechanism whereby the ill-posedness may be shut-off as large velocity gradients appear in ill-posed regions.

The stability properties of these equations is similar to that of the critical state plasticity studied by Schaeffer [13]. Indeed, the parameter μ (equation 33) here plays a role similar to the dilation angle in CST. However, the equations proposed here are considerably simpler than the CST equations and may be a simpler system in which to study shear banding (the CST equations, however, will certainly provide a better model for granular flows). For instance, it may be possible to study the non-linear stability of this system to obtain a deeper understanding of the development of shear bands and their relationship to ill-posed behaviour.

Acknowledgements

The author thanks Dr Graham Weir and Dr Roger Young for their help and guidance.

Approximate radial solutions

For wedge-shaped hoppers Brennen and Pearce [2] and Kaza and Jackson [8], have examined steady-state plane-strain flows by expanding the velocities and the pressure in powers of $(\tan \alpha_w)$ where α_w is the wall-angle of the wedge-shaped hopper. The steady-state equations are then solved order by order using a radial-flow ansatz. The first order terms in these expansions are similar to the

radial solutions of Jenike for the quasistatic ($F/r \ll 1$) steady-state equations (8) and (9). These approximations contain corrections due to the inclusion of the inertial terms when $F/r \ll 1$. Working in polar coordinates (r, θ) where the hopper walls lie at $r = r_w$ in the plane and using the Sokolovskii parameterization of the stresses ([16]), the ansatz goes as follows:

$$p = p_0(r) + O\left(\frac{r^2}{w^2}\right); \quad (40)$$

$$= \frac{1}{w} + O\left(\frac{r^3}{w^3}\right); \quad (41)$$

where σ_r is related to the stresses by

$$\sigma_r = \frac{2}{r} \frac{dp}{dr}.$$

The leading order terms in r are then given by:

$$p_0(r) = \frac{5_0}{1 - \sin^2 \theta} \frac{F^2}{w + 2} \frac{1}{w - 1} \frac{r}{r_0} + \frac{r - r_0}{w - 1} \frac{F^2}{w + 2} \frac{r_0}{r} \quad (42)$$

$$\frac{1}{w} = \frac{1}{w}; \quad (43)$$

where r_w is the value of r at the wall (determined by the boundary condition (7)),

$$w = \frac{2 \sin^2 \theta}{(1 - \sin^2 \theta)} (1 + \frac{r_w}{r}) :$$

and

$$F^2 = \frac{w + 2}{w - 1} \frac{B}{C} \frac{1}{1 - \frac{r_0}{r_1}} \frac{r_0}{r_1} \frac{1}{w + 2} \frac{1}{A} :$$

Here $r = r_0$ and $r = r_1$ are the arcs along which the average stress vanishes (the outflow and inflow respectively). The corresponding terms in the velocity fields are also radial (to order $(r/w)^2$):

$$u = \frac{p}{g r_0 F} \frac{1}{w - 1} \frac{2}{w} \frac{r_0}{r} \quad (44)$$

$$v = 0; \quad (45)$$

where u and v are the radial and angular components of the velocity respectively.

References

- [1] P. Bastian, K. Birken, K. Johannsen, S. Lang, K. Eckstein, N. Neuss, H. Rentz-Reichert, and C. Wieners. Ug - a flexible software toolbox for solving partial differential equations. Computing and Visualization in Science, 127(40), 1997.

- [2] C. Brennen and J. C. Pearce. Granular material flow in two-dimensional hoppers. *Journal of Applied Mechanics*, 45:43, 1978.
- [3] A. Drescher. On the criteria for mass flow in hoppers. *Powder Technology*, 73:251{260, 1992.
- [4] D. C. Ducker and W. Prager. *Q. Appl. Math.*, 10:157, 1952.
- [5] P. A. G renaud and J. V. Matthews. On the computation of steady hopper flows: I, stress determination for coulomb materials. Technical Report CRSC TR 99-35, Center for Research in Scientific Computing, North Carolina State University, Raleigh, 1999.
- [6] A. Jenike. Gravity flow of bulk solids. Technical report, Utah Engineering Experimental Station, University of Utah, Salt Lake City, 1964.
- [7] S. M. H. Karimian and G. E. Schneider. Pressure-based control-volume finite element method for flow at all speeds. *AIAA Journal*, 33(9):1611, 1995.
- [8] K. R. Kaza and R. Jackson. The rate of discharge of coarse granular material from a wedge-shaped mass flow hopper. *Powder Technology*, 33:223, 1982.
- [9] H. B. Muhlhaupt and F. Oka. Dispersion and wave propagation in discrete and continuous models for granular materials. *Journal of Solids and Structures*, 33:2841{2858, 1996.
- [10] R. M. Nedderman. *Statics and Kinematics of Granular Materials*. Cambridge University Press, London, 1992.
- [11] S. V. Patankar. *Numerical Heat Transfer and Fluid Flow*. Hemisphere, Washington D C., 1980.
- [12] D. G. Schaefer. Instability in the evolution equations describing incompressible granular flow. *Journal of Differential Equations*, 66:19, 1987.
- [13] D. G. Schaefer. Instability and ill-posedness in the deformation of granular materials. *International Journal for Numerical and Analytical Methods in Geomechanics*, 14:253{278, 1990.
- [14] D. G. Schaefer. A mathematical model for localization in granular flow. *Proceedings of the Royal Society of London A*, 436:217{250, 1992.
- [15] G. E. Schneider and M. J. Raw. Control-volume finite-element method for heat transfer and fluid flow using colocated variables - 1. computational procedure. *Numerical Heat Transfer*, 11:363, 1987.
- [16] V. V. Sokolovskii. *Statics of Granular Materials*. Pergamon, Oxford, 1965.

- [17] R. B. Thorpe. An experimental clue to the importance of dilation in determining the flow rate of a granular material from a hopper or bin. *Chemical Engineering Science*, 47:4295-4303, 1992.
- [18] K. C. Valanis and J. F. Peters. Ill-posedness of the initial and boundary value problems in non-associative plasticity. *Acta Mechanica*, 114:1-25, 1996.